

Magnetoelectric and Raman spectroscopic studies of monocrystalline MnCr₂O₄G. T. Lin,^{1,2} Y. Q. Wang,^{2,3} X. Luo,^{1,*} J. Ma,^{4,5} H. L. Zhuang,⁶ D. Qian,^{5,7} L. H. Yin,¹ F. C. Chen,^{1,2} J. Yan,^{1,2} R. R. Zhang,³ S. L. Zhang,³ W. Tong,³ W. H. Song,¹ P. Tong,¹ X. B. Zhu,¹ and Y. P. Sun^{1,3,7,†}¹Key Laboratory of Materials Physics, Institute of Solid State Physics, Chinese Academy of Sciences, Hefei 230031, China²University of Science and Technology of China, Hefei 230026, China³High Magnetic Field Laboratory, Chinese Academy of Sciences, Hefei 230031, China⁴Quantum Condensed Matter Division, Oak Ridge National Laboratory, Oak Ridge, Tennessee 37831, USA⁵Department of Physics and Astronomy, Shanghai Jiao Tong University, Shanghai 200240, China⁶School for Engineering of Matter, Transport & Energy, Arizona State University, Tempe, Arizona 85287, USA⁷Collaborative Innovation Center of Advanced Microstructures, Nanjing University, Nanjing 210093, China

(Received 15 December 2017; published 12 February 2018)

MnCr₂O₄ that exhibits spin frustration and complex spiral spin order is of great interest from both fundamental as well as application-oriented perspectives. Unlike CoCr₂O₄, whose ground state presents the coexistence of commensurate spiral spin order (CSSO) and ferroelectric order, MnCr₂O₄ shows no multiferroicity. One reason is that the spiral spin order is highly sensitive to the oxygen concentration in MnCr₂O₄. Here, we have successfully grown high-quality single-crystalline MnCr₂O₄ by the chemical vapor transport method. We observe a first-order magnetic transition from the incommensurate spiral spin order (ICSSO) at 19.4 K to the CSSO at 17.4 K. This magnetic transition is verified by magnetization, specific heat, and magnetoelectric measurements, which also confirm that the ground state exhibits the coexistence of the CSSO and magnetoelectricity below 17.4 K. Interestingly, the temperature evolution of Raman spectra between 5.4 and 300 K suggests that the structure remains the same. We also find that the phase-transition temperature of the CSSO decreases as applied magnetic field increases up to 45 kOe.

DOI: [10.1103/PhysRevB.97.064405](https://doi.org/10.1103/PhysRevB.97.064405)**I. INTRODUCTION**

Insulators with spiral spin order, offering immense potential in low-loss memory devices, have attracted significant interest due to their multiferroicity (MF) in which the dielectric and magnetic polarizations can be manipulated by applying either magnetic fields or electric ones [1–9]. In these MFs, spinel compounds with cubic structure are an important class of materials and their electronic properties have drawn great attention due to their colossal magnetocapacitance and spontaneous dielectric polarization in the magnetically ordered state [1,2,10–16]. The appearance of MF is associated with either noncollinear spiral spin order or off-centering of magnetic ions from their symmetric site positions in the lattice [1,2,10–17]. Nevertheless, single-crystalline MnCr₂O₄, showing a complex spiral spin order similar to CoCr₂O₄, has not shown MF effects up to now [1,2,15–30].

MnCr₂O₄ crystallizes in a cubic spinel structure with $Fd\bar{3}m$ space group [shown in Fig. 5(a)], where magnetic Mn²⁺ ($3d^5$, $S = 5/2$) and Cr³⁺ ($3d^3$, $S = 3/2$) ions occupy the tetrahedral and octahedral sites, respectively. A long-range ferrimagnetic spin order (LFIM) appears below $T_C = 41$ – 52 K, followed by transition into a short-range spiral spin order at $T_S = 14$ – 20 K [15,18–23,25,26]. Compared with CoCr₂O₄, an incommensurate spiral spin order to commensurate spiral spin order

transition remains to be clarified in MnCr₂O₄ [1,2,15–23,25–31]. And, it is obvious that the spiral spin order may be very sensitive to oxygen content [31], which may be one of the reasons that the magnetic ground state of MnCr₂O₄ is as yet in dispute. Therefore, firstly, the high-quality single-crystalline MnCr₂O₄ is successfully grown by the chemical vapor transport method (CVT). Then, we present a detailed investigation of magnetic ground state in single-crystalline MnCr₂O₄. We find that a first-order transition from ICSSO to CSSO with magnetoelectricity occurs at $T_L = 17.4$ K, indicating strong spin-lattice coupling. Interestingly, the temperature evolution of Raman spectrum between 5.4 and 300 K indicates that there is no structural phase change in MnCr₂O₄.

II. EXPERIMENTAL AND THEORETICAL DETAILS

Samples of single-crystalline MnCr₂O₄ were grown by the CVT, with CrCl₃ powders as the transport agent. Experimental details concerning the preparation of MnCr₂O₄ were given in Ref. [19]. The x-ray diffraction (XRD) data indicated that the powders were single phase with cubic structure (see Supplemental Material [32]). We measured the specific heat (SH) using the Quantum Design physical properties measurement system (PPMS-9T) and characterized the magnetic properties by the magnetic property measurement system (MPMS-XL5). The x-ray photoelectron spectra (XPS) were measured in a Thermo ESCALAB 250 spectrometer using Al K α x ray at 1486.6 eV as the excitation source (see Supplemental Material [32]). A plate with the (111) plane of 0.5×0.5 mm² was

*xluo@issp.ac.cn

†ypsun@issp.ac.cn

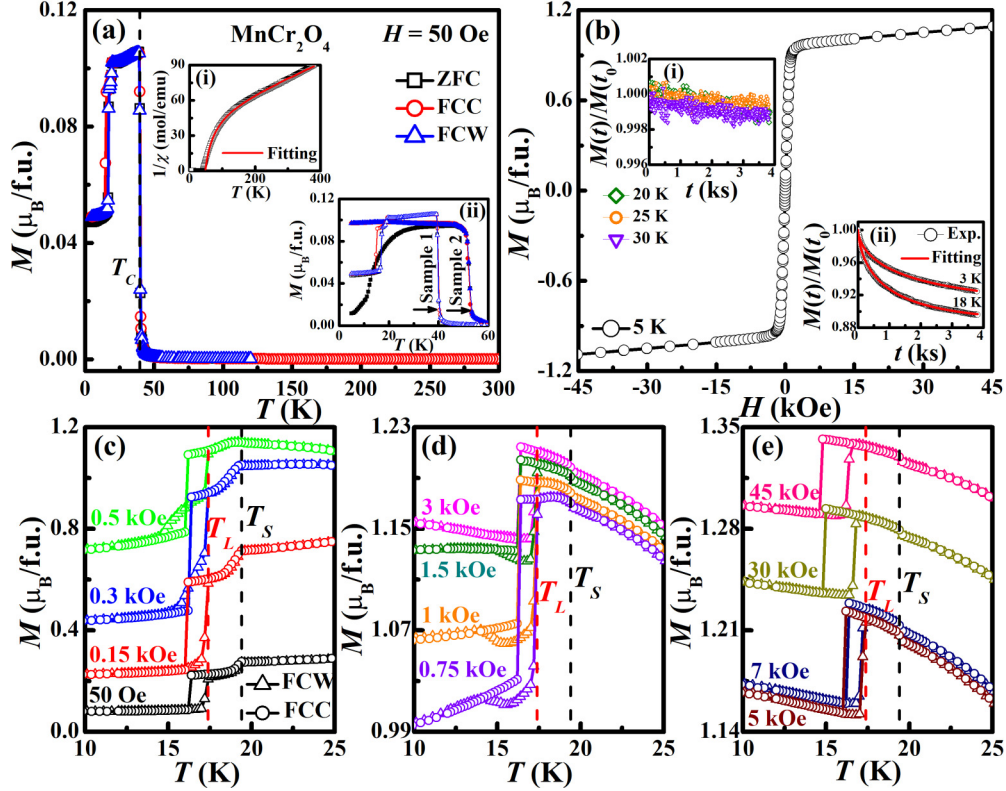


FIG. 1. (a) Temperature-dependent magnetization $M(T)$ of MnCr_2O_4 under the ZFC, FCC, and FCW with an applied magnetic field $H = 50$ Oe, parallel to the $\langle 111 \rangle$ direction. The inset (i) shows the temperature-dependent inverse susceptibility $\chi(T)^{-1}$. The red solid line is the fitting result according to Eq. (1). The inset (ii) shows the temperature-dependent magnetization $M(T)$ measurements of samples 1 and 2 with $H = 50$ Oe, parallel to the $\langle 111 \rangle$ direction. (b) The isothermal magnetization curves $M(H)$ at 5 K, parallel to the $\langle 111 \rangle$ direction. The insets (i) and (ii) present the time-dependent magnetization $M(t)$ under FCC mode below T_C . (c)–(e) The enlarged view of the $M(T)$ under FCC and FCW modes with different applied magnetic field, parallel to the $\langle 111 \rangle$ plane.

polished from the single crystal. The specimen was cooled down to 2 K with an applied electric field $E = 0$ V along $[111]$ at different applied magnetic fields parallel to the $\langle 111 \rangle$ plane. Raman-scattering experiments were conducted by using the 780-nm laser line in a DXR Raman Microscope (Thermo Scientific). The scattering light was collected by using a single exposure of the charge-coupled device with a spectral resolution of 1 cm^{-1} . Low-temperature Raman spectra were obtained on a Raman Microscope (Horiba JY T64000) equipped with a Janis ST-500 microscopy cryostat.

We used the Vienna *Ab initio* Simulation Package (VASP) [33] to calculate the force constants and Raman spectrum [34] of MnCr_2O_4 . Plane waves with a cutoff energy of 500 eV were employed to model the valence electrons. We used the potentials based on the projector augmented-wave method [35,36]. We also used the Perdew-Burke-Ernzerhof functional [37] to describe the exchange-correlation interactions. Similar to a previous theoretical study [38], the Coulomb interactions between d orbitals of Mn and Cr atoms were treated with Dudarev's effective U - J parameters [39] of 3.0 and 5.0 eV, respectively. We computed the force constants using $3 \times 3 \times 3$ supercells and these force constants were postprocessed by the PHONOPY program [40] to obtain the phonon spectrum of MnCr_2O_4 . K -point meshes based on the Monkhorst-Pack scheme [41] were $6 \times 6 \times 6$ and $2 \times 2 \times 2$ for the unit cell and supercells, respectively.

III. RESULTS AND DISCUSSION

Figure 1(a) shows the temperature-dependent magnetization $M(T)$ of MnCr_2O_4 under the zero-field-cooled warming (ZFC), field-cooled cooling (FCC), and field-cooled warming (FCW) modes with applied magnetic field $H = 50$ Oe, parallel to the $\langle 111 \rangle$ direction. We observe a paramagnetic-ferrimagnetic (PM-FIM) transition that occurs at T_C of 40 K, as determined by the derivative of the magnetization. This temperature is close to the values of 41–52 K reported previously [15,18–23,25,26]. For a FIM system, the temperature-dependent inverse susceptibility $\chi(T)^{-1}$ above T_C can be described by the hyperbolic behavior characteristic of ferrimagnets resulting from the mean-field theory [25,42].

$$\frac{1}{\chi} = \frac{T - \theta}{C} - \frac{\zeta}{T - \theta'}, \quad (1)$$

where C is the Curie constant, θ is the Weiss temperature, the first term is the hyperbolic high- T asymptote that has a Curie-Weiss (CW) form, and the second term is the hyperbolic low- T asymptote. The fitted $\chi(T)^{-1}$ for MnCr_2O_4 by Eq. (1) is shown by the red curve in the inset of Fig. 1(a) using the $C = 8.51 \text{ emu K/mol}$, $\theta = -410.9 \text{ K}$, $\zeta = 1449.2 \text{ mol K/emu}$, and $\theta' = 20.6 \text{ K}$. The effective magnetic moment is determined to be $\mu_{\text{eff}} \sim 8.25 \mu_B$ ($\mu_{\text{eff}} = \sqrt{3k_B C / N_A \mu_B}$), which is close to the theoretical value

expected for high-spin Cr^{3+} ($S = 3/2$) and Mn^{2+} ($S = 5/2$) [25]. The high ratio of $|\theta|/T_C \sim 10$ indicates significant magnetic frustration due to competing J_{CrCr} , J_{MnMn} , and J_{MnCr} exchange interactions that establish the spiral spin order at low temperatures [21,22,25]. Figure 1(b) shows the isothermal magnetization $M(H)$ at 5 K and the $M(H)$ curve presents almost no coercive force for single-crystalline MnCr_2O_4 . Above about 3 kOe, the magnetization increases linearly with applied field exhibiting a typical FIM behavior (parallel to the $\langle 111 \rangle$ direction). In the insets (i) and (ii) of Fig. 1(b), time-dependent magnetization $M(t)$ of MnCr_2O_4 under FCC mode is recorded below T_C . The sample is dropped to the desired temperatures from well above T_C in 100 Oe and decay of $M(t)$ is recorded with t . The $M(t)$ is fitted with the modified stretched exponential function [15]

$$M(t) = M_0 - M_g \exp[-(t/\tau)^\beta], \quad (2)$$

where the M_0 and M_g are the ferromagnetic and exponential components of $M(t)$, respectively. β is an exponent with the range $0 < \beta < 1$. The fitted curve using Eq. (2) is displayed in the inset of Fig. 1(b). The values of M_g/M_0 , τ , and β are 90.3%, 2004 s, and 0.58, respectively, at 3 K and 88.7%, 972 s, and 0.64, respectively, at 18 K. $\beta < 1$ indicates the relaxation mechanism with the spin-glass-like behavior (SG-like) [15]. Compared to the $M(t)$ with no the relaxation above $T_S = 19.4$ K, the significant relaxation of $M(t)$ is observed below T_S , which does not agree with the previous reports that the relaxation with the SG-like can be also seen between T_C and T_S [15,18–21]. One of the reasons for the difference is attributable to the defects caused by oxygen vacancies in the different MnCr_2O_4 samples, which can be confirmed by the inset (ii) of Fig. 1(a). Here, we compare the two selected samples named sample 1 (this work) and sample 2 (single-crystalline MnCr_2O_4 of Refs. [18,19]). We observe a PM-FIM transition that occurs at T_C of 39.5 K (sample 1) and 52 K (sample 2), as determined by the derivative of the magnetization. For sample 2, one can see the phenomena as follows: the anomaly at $T_S \approx 18$ K in the FCC curve, a weak thermal hysteresis observed in the FC magnetization, and reentrant-spin-glass-like characteristic temperature $T_i \approx 47$ K, which is consistent with the previous reports [15,18,19,21]. In contrast to the sample 2, there is a lower PM-FIM transition temperature T_C , an anomaly independent of the applied magnetic field at T_S , and a first-order transition at T_L for sample 1 (for more details see Supplemental Material [32]).

In order to show clearly the low-temperature phase transitions, we plot the enlarged view of the $M(T)$ under FCC and FCW modes with different applied magnetic field, parallel to the (111) plane [Figs. 1(c)–1(e)]. By analogy with CoCr_2O_4 [17,21,27,29], it is noticed that all $M(T)$ curves show a steplike kink at the ICSSO transition at $T_S = 19.4$ K. If the temperature further decreases, the $M(T)$ curves exhibit a second anomaly at the transition into the CSSO at $T_L = 17.4$ K with a hysteresis under FCC and FCW modes, confirming the first-order magnetic phase transition. With an increasing magnetic field, the anomaly in the magnetization at T_L shifts to lower temperatures, whereas the position of the anomaly at T_S remains unchanged.

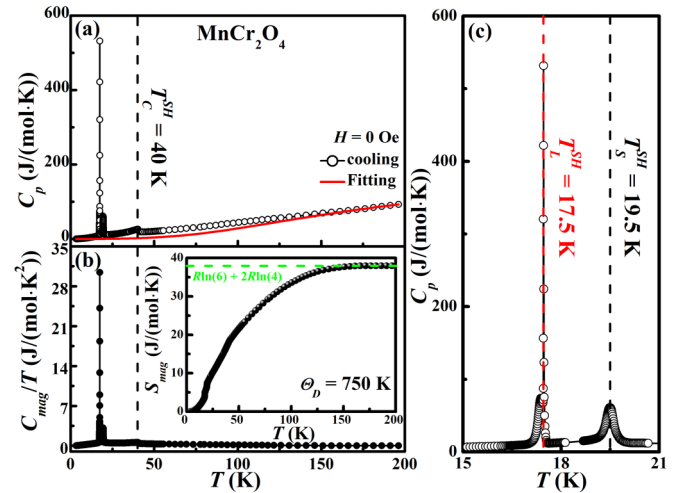


FIG. 2. (a) Specific heat C_p as a function of T for MnCr_2O_4 and the fitted $C_V^{\text{Debye}}(T)$ using Eqs. (3) and (4). (b) Temperature-dependent magnetic specific heat $C_{\text{mag}}(T)$. The inset shows the magnetic entropy $S_{\text{mag}}(T)$. The red dashed line refers to $S_{\text{mag}}(T \rightarrow \infty)$ calculated with the magnetic moment $S = 5/2$ for Mn^{2+} and $S = 3/2$ for Cr^{3+} . (c) The enlarged view of the $C_p(T)$ under cooling and warming modes with $H = 0$ Oe.

Figure 2(a) shows the variation of the zero-field SH $C_p(T)$ with temperature under cooling mode. The sharp anomaly in $C_p(T)$ at $T_C^{\text{SH}} = 40$ K corresponds to the FIM transition temperature, followed by a transition into an ICSSO at $T_S^{\text{SH}} = 19.5$ K. The most striking feature with a sharp peak at $T_L^{\text{SH}} = 17.5$ K is ascribed to the CSSO. Since MnCr_2O_4 is an insulator, the electronic contribution to the heat capacity is not considered. The C_{mag} can be calculated by the following equations [42]:

$$C_{\text{mag}}(T) = C_p(T) - nC_V^{\text{Debye}}(T), \quad (3)$$

and

$$C_V^{\text{Debye}}(T) = 9R \left(\frac{T}{\Theta_D} \right)^3 \int_0^{\Theta_D/T} \frac{x^4 e^x}{(e^x - 1)^2} dx, \quad (4)$$

where R is the molar gas constant, Θ_D is the Debye temperature, and $n = 7$ is the number of atoms per formula unit. The sum of Debye functions accounts for the lattice contribution to SH. We can extract the magnetic contribution $C_{\text{mag}}(T)$ from the measured SH of MnCr_2O_4 . The fitted $C_p(T)$ by Eqs. (3) and (4) over the temperature range from about 3 to 200 K is shown by the red curve in Fig. 2(a) using the Debye temperature, $\Theta_D = 750$ K. This value compares well to the Debye temperature in ferrites [43]. The $C_{\text{mag}}(T)$ curve exhibits three clear features, indicative of three phase transitions, as displayed in Fig. 2(b). The magnetic entropy $S_{\text{mag}}(T)$ is calculated by

$$S_{\text{mag}}(T) = \int_0^T \frac{C_{\text{mag}}(T)}{T} dT. \quad (5)$$

The inset of Fig. 2(b) shows the temperature dependence of $S_{\text{mag}}(T)$. The entropy of MnCr_2O_4 per mole with completely

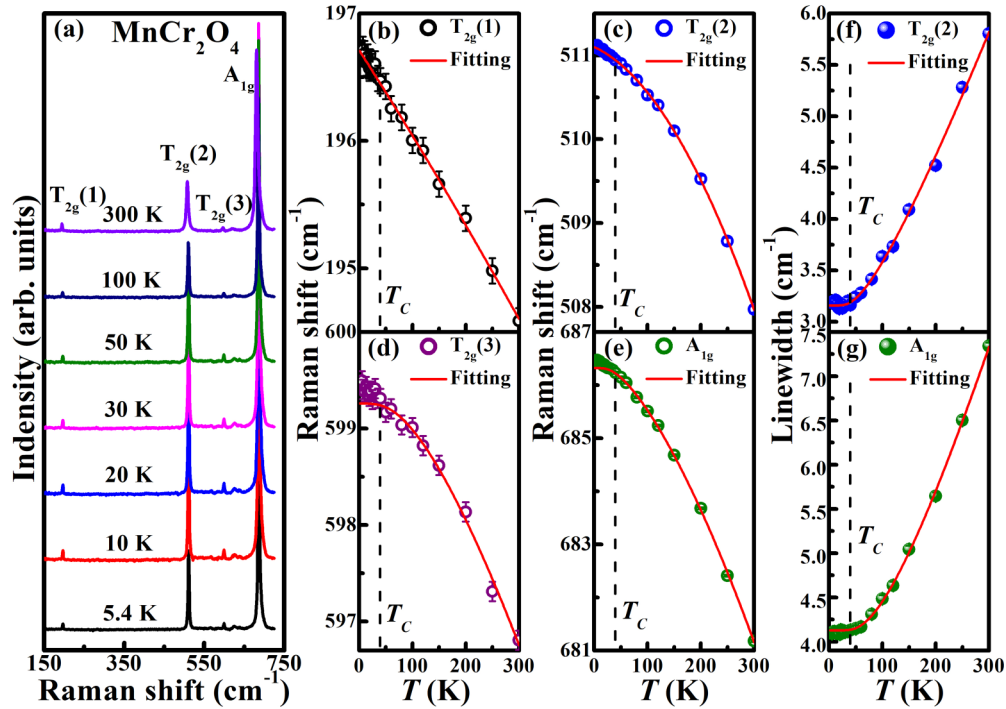


FIG. 3. (a) Temperature-dependent Raman spectra of MnCr_2O_4 ; Temperature-dependent Raman phonon frequencies of (b) $T_{2g}(1)$, (c) $T_{2g}(2)$, (d) $T_{2g}(3)$, and (e) A_{1g} modes. The red solid lines are the anharmonic contributions to the phonon frequencies fitted by Eq. (7). Temperature-dependent linewidth of (f) $T_{2g}(2)$ and (g) A_{1g} modes.

disordered spins S is

$$S_{\text{mag}}(T \rightarrow \infty) = R \ln(2S_{\text{Mn}^{2+}} + 1) + 2R \ln(2S_{\text{Cr}^{3+}} + 1). \quad (6)$$

Using $S = 5/2$ for Mn^{2+} and $S = 3/2$ for Cr^{3+} , we obtain $S_{\text{mag}}(T \rightarrow \infty)$ of $37.9 \text{ J}/(\text{mol} \cdot \text{K})$. However, we observe the S_{mag} is $17.8 \text{ J}/(\text{mol} \cdot \text{K})$ at T_C^{SH} , which is only 47% of the value expected for $S_{\text{mag}}(T \rightarrow \infty)$. Note that there is an error of about 10% [44] in our measurement due to the fitting of the optical phonon contributions at high temperatures. In spite of this small error, our result indicates the strong dynamic short-range spin interactions above T_C . In addition, we plot the enlarged view of the $C_p(T)$, as shown in Fig. 2(c). There are two extremely sharp peaks at T_S^{SH} and T_L^{SH} , indicating the first-order transition (see Supplemental Material [32]).

To determine if there is a structural transition near the magnetic transitions in MnCr_2O_4 , the temperature evolution of Raman spectrum in the energy range $150\text{--}720 \text{ cm}^{-1}$ is studied in detail between 5.4 and 300 K, as shown in Fig. 3(a). MnCr_2O_4 has a cubic ($Fd\bar{3}m$) structure with five Raman-active modes which are classified as $\Gamma_{\text{Raman}} = 3T_{2g} + A_{1g} + E_g$ [45]. The spectra in Fig. 3(a) show no indication of the splitting of the T_{2g} and A_{1g} between 5.4 and 300 K at least to within the resolution of this experiment, indicating no structure change. This result is in agreement with diffraction studies and optical conductivity spectra of MnCr_2O_4 [15,21,26]. And, we display the calculated phonon and Raman spectra of MnCr_2O_4 (see Supplemental Material [32]). One can observe the same Raman-active modes as seen in the experiment. In particular, the A_{1g} mode exhibits the largest Raman intensity, which is consistent with our experimental observation. In addition, the indistinguishable

phonon at $\omega = 453 \text{ cm}^{-1}$, ascribed to E_g symmetry, may be the noise in the spectrum, which appears to be missing since its intensity is very weak in Fig. 3(a). To explore possible signatures of subtle spin-phonon coupling, the temperature-dependent phonon frequencies and linewidth (full width at half maximum), determined from fitting the peak to a Lorentzian, are plotted in Figs. 3(b)–3(g). Under the assumption that decay occurs to two phonons of frequencies ω_1 and ω_2 and three identical phonons of frequency $\omega/3$ [45–47], the phonon frequencies increase with decreasing temperature up to T_C due to the anharmonic effect, which can be fitted by the equation [47]

$$\omega_{\text{anh}} = \omega_0 + A \left(1 + \frac{1}{e^{x_1} - 1} + \frac{1}{e^{x_2} - 1} \right) + B \left(1 + \frac{3}{e^{x_3} - 1} + \frac{3}{(e^{x_3} - 1)^2} \right), \quad (7)$$

where ω_0 , A , and B are adjustable parameters, $x_1 = hc\omega_1/k_B T$, $x_2 = hc\omega_2/k_B T$, and $x_3 = hc\omega/3k_B T$. h , c , k_B , and T denote the Planck's constant, speed of light, Boltzmann's constant, and temperature, respectively. This model describes adequately the temperature dependence of $T_{2g}(1)$ and $T_{2g}(2)$ phonon modes between 5.4 and 300 K, as shown in Figs. 3(b) and 3(c). The magnetic order below T_C , however, results in an very weak anomalous hardening of $T_{2g}(3)$ and A_{1g} phonon modes, as evidenced in Figs. 3(d) and 3(e). It may be due to the fact that five modes (A_{1g} , E_g , $3T_{2g}$) of Raman-active have a weak response to the spin-lattice coupling. Therefore, the study of infrared spectroscopy is necessary in the future. Nevertheless, our results confirm that the cubic symmetry of the lattice is preserved even in the magnetically ordered ground state in MnCr_2O_4 .

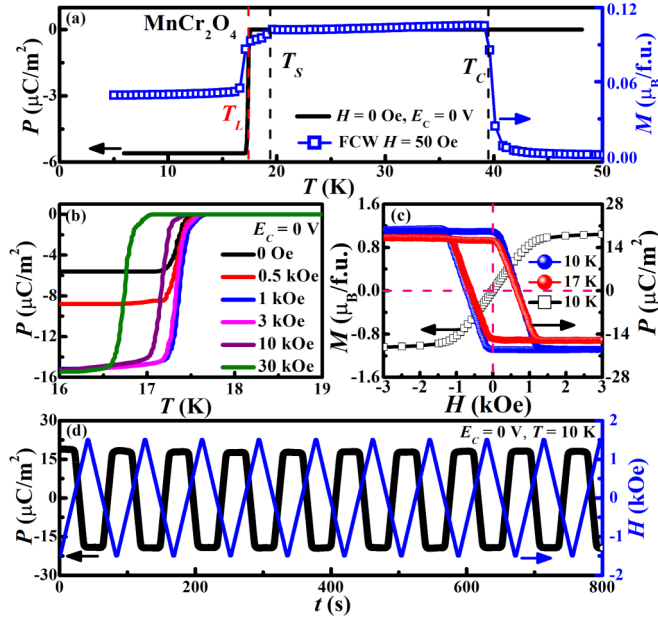


FIG. 4. (a) Temperature-dependent electric polarization $P(T)$ and $M(T)$ along the [111] direction. (b) $P(T)$ along the [111] direction around the T_L with different applied field. (c) The $M(H)$ at 10 K, parallel to the $\langle 111 \rangle$ direction. The field-dependent electric polarization $P(H)$ at 10 and 17 K, respectively, parallel to the $\langle 111 \rangle$ direction. (d) The synchronous reversal of the spontaneous M and P between $+1.5$ and -1.5 kOe at 10 K.

Figure 4(a) shows temperature-dependent electric polarization $P(T)$ and $M(T)$ along the [111] direction, in which the onset of pyroelectric current corresponds with the CSSO transition at $T_L = 17.4$ K. Figure 4(b) displays how $P(T)$ depends on the different H at $E_C = 0$ V, showing a slight decreasing tendency of T_L with increasing H . And, the intensity of $P(T)$, tending to be saturated above about $H = 1$ kOe, increases rapidly with increasing H . In Fig. 4(c), one can observe the field-dependent electric polarization $P(H)$ at 10 and 17 K, respectively, in comparison with the $M(H)$ curve at 10 K. The synchronous reversal of the spontaneous M and P can be more directly confirmed by the continuous sweep field between $+1.5$ and -1.5 kOe at 10 K [see Fig. 4(d)]. The strikingly reversible and reproducible variation of the P is observed without any noticeable decay in its magnitude. By combining this highly reproducible P reversal with the ability to leave a permanent "imprint" in the polarization with an applied magnetic field demonstrated in Figs. 4(b) and 4(d), one can envision that the low-field magnetoelectric effect has the promise of practical device applications, namely, a nonvolatile memory [48] where information is stored as electrically detectable and electrically controllable spin helicity.

As we know, a spontaneous electric polarization can appear when the spins form a transverse-spiral (cycloidal) modulation along a specific crystallographic direction and the spin rotation axis is not parallel to the propagation vector. The direction of the P can be expressed by the equation [3,5,49–51]

$$\mathbf{P} = \gamma \sum_{(i,j)} \mathbf{e}_{ij} \times (\mathbf{S}_i \times \mathbf{S}_j). \quad (8)$$

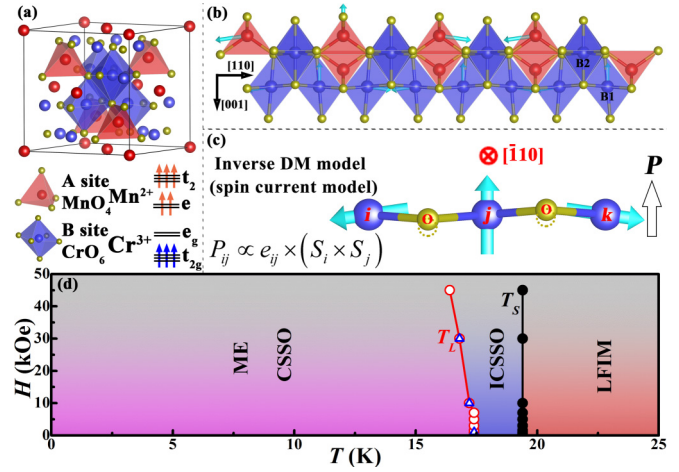


FIG. 5. (a) Schematic structure of spinel MnCr_2O_4 . The electron configuration of Mn^{2+} and Cr^{3+} ions, located at the center of tetrahedral and octahedral O^{2-} cages, respectively. Here, the splitting due to the local crystal field of the ions in the cubic phase and the effect of Hund coupling are only taken into account. (b) Low-temperature magnetic structure of spinel MnCr_2O_4 viewed along $[1\bar{1}0]$ direction. (c) The spin (\mathbf{S}_i and \mathbf{S}_j) canting between the two sites (i and j) and the direction of induced polarization \mathbf{P} . (d) Schematic low-temperature phase diagram of MnCr_2O_4 . The open circles and triangles refer to the phase-transition temperature obtained by $M(T)$ and $P(T)$ curves along the [111] directions, respectively.

Here, γ is a coefficient proportional to the spin-orbit coupling and superexchange interactions as well as spin-lattice coupling, \mathbf{e}_{ij} is along the propagation vector of a spiral structure, and $(\mathbf{S}_i \times \mathbf{S}_j)$ is parallel to the spin rotation axis. This model is termed the inverse Dzyaloshinskii-Moriya (DM) model or the spin-current model. The MF effect in many compounds, i.e., $R\text{MnO}_3$ ($R = \text{Tb}, \text{Dy}, \text{etc.}$) [52,53], CoCr_2O_4 [1,2,16], and so on, can be explained by Eq. (8). In addition, neutron scattering measurements have proved that the magnetic ground state of MnCr_2O_4 shows the coexistence of the conical spin order and LFIM, where the spontaneous magnetization vector is parallel to $[1\bar{1}0]$ or equivalent directions [21–24]. The conical spin order can be seen as composed of the cycloidal component and the ferrimagnetic component in this structure. Hence, as shown in Figs. 5(b) and 5(c), the magnetoelectric effect of MnCr_2O_4 can also be categorized into cycloidal spiral origin based on Eq. (8), which has been confirmed by the polycrystalline MnCr_2O_4 [15]. It should be mentioned that the spin rotation axis is parallel to the direction of ferrimagnetic component of the conical spin order, namely the $[1\bar{1}0]$ axis. Then, according to Eq. (8), the spontaneous polarization vector is expected to lie along the $[001]$ axis. As mentioned above, we only test the magnetoelectric properties along the [111] direction, namely, the normal direction of easy-growth plane due to the extremely small size in single-crystalline MnCr_2O_4 . However, our results also verify that there is a strong magnetoelectric coupling in MnCr_2O_4 . In addition, the ferroelectricity in MnCr_2O_4 still needs further investigation. This is due to the fact that the reverse electric field cannot reverse the direction of the P (see Supplemental Material [32]).

IV. CONCLUSION

Finally, based on the magnetization, SH, and magnetoelectric measurements, we plot the low-temperature phase diagram of MnCr_2O_4 [see Fig. 5(d)]. The first-order transition from the LFIM to the ICSSO at $T_S = 19.4$ K is almost field independent. The subsequent transition to the CSSO decreases with the external magnetic field at least up to 45 kOe, corresponding to the onset of spontaneous electric polarization with the external magnetic field. In addition, the temperature evolution of Raman spectrum between 5.4 and 300 K indicates that there is no structural phase change in MnCr_2O_4 .

ACKNOWLEDGMENTS

This work was supported by the National Key Research and Development Program under Contracts No. 2016YFA0401803

and No. 2016YFA0300404, the Joint Funds of the National Natural Science Foundation of China and the Chinese Academy of Sciences' Large-Scale Scientific Facility under Contracts No. U1432139 and No. U1532153, the National Natural Science Foundation of China under Contracts No. 11674326 and No. 11404339, Key Research Program of Frontier Sciences, CAS (QYZDB-SSW-SLH015), and the Nature Science Foundation of Anhui Province under Contract No. 1508085ME103. This work used computational resources of the Texas Advanced Computing Center under Contract No. TG-DMR170070. H.L.Z. acknowledge the start-up funds from Arizona State University. G.T.L. thanks Dr. C. Sun from University of Wisconsin-Madison for her assistance in editing the revised manuscript.

G.T.L. and Y.Q.W. contributed equally to this work.

-
- [1] Y. Yamasaki, S. Miyasaka, Y. Kaneko, J. P. He, T. Arima, and Y. Tokura, *Phys. Rev. Lett.* **96**, 207204 (2006).
- [2] Y. J. Choi, J. Okamoto, D. J. Huang, K. S. Chao, H. J. Lin, C. T. Chen, M. van Veenendaal, T. A. Kaplan, and S. W. Cheong, *Phys. Rev. Lett.* **102**, 067601 (2009).
- [3] Y. Tokura and S. Seki, *Adv. Mater.* **22**, 1554 (2010).
- [4] M. Mostovoy, *Phys. Rev. Lett.* **96**, 067601 (2006).
- [5] H. Katsura, N. Nagaosa, and A. V. Balatsky, *Phys. Rev. Lett.* **95**, 057205 (2005).
- [6] R. Ramesh and N. A. Spaldin, *Nat. Mater.* **6**, 21 (2007).
- [7] S.-W. Cheong and M. Mostovoy, *Nat. Mater.* **6**, 13 (2007).
- [8] T. Kimura, *Annu. Rev. Mater. Res.* **37**, 387 (2007).
- [9] M. Fiebig, T. Lottermoser, D. Meier, and M. Trassin, *Nat. Rev. Mater.* **1**, 16046 (2016).
- [10] V. Gnezdilov, P. Lemmens, Y. G. Pashkevich, C. Payen, K. Y. Choi, J. Hemberger, A. Loidl, and V. Tsurkan, *Phys. Rev. B* **84**, 045106 (2011).
- [11] Y. O. H. Murakawa, K. Ohgushi, S. Ishiwata, and Y. Tokura, *J. Phys. Soc. Jpn.* **77**, 043709 (2008).
- [12] S. Weber, P. Lunkenheimer, R. Fichtl, J. Hemberger, V. Tsurkan, and A. Loidl, *Phys. Rev. Lett.* **96**, 157202 (2006).
- [13] J. Hemberger, P. Lunkenheimer, R. Fichtl, H. A. Krug von Nidda, V. Tsurkan, and A. Loidl, *Nature (London)* **434**, 364 (2005).
- [14] N. Nugroho, A. A. Blake, G. R. Palstra, and T. T. M. Palstra, *J. Phys.: Condens. Matter* **22**, 075902 (2010).
- [15] K. Dey, S. Majumdar, and S. Giri, *Phys. Rev. B* **90**, 184424 (2014).
- [16] T.-h. Arima, Y. Yamasaki, T. Goto, S. Iguchi, K. Ohgushi, S. Miyasaka, and Y. Tokura, *J. Phys. Soc. Jpn.* **76**, 023602 (2007).
- [17] V. Tsurkan, S. Zherlitsyn, S. Yasin, V. Felea, Y. Skourski, J. Deisenhofer, H. A. Krug von Nidda, J. Wosnitza, and A. Loidl, *Phys. Rev. Lett.* **110**, 115502 (2013).
- [18] G. T. Lin, W. Tong, X. Luo, F. C. Chen, L. H. Yin, Y. Q. Wang, L. Hu, Y. M. Zou, L. Yu, W. H. Song, and Y. P. Sun, *J. Alloys Compd.* **711**, 250 (2017).
- [19] G. T. Lin, X. Luo, Q. L. Pei, F. C. Chen, C. Yang, J. Y. Song, L. H. Yin, W. H. Song, and Y. P. Sun, *RSC Adv.* **6**, 56839 (2016).
- [20] D. Y. Yoon, S. Lee, Y. S. Oh, and K. H. Kim, *Phys. Rev. B* **82**, 094448 (2010).
- [21] K. Tomiyasu, J. Fukunaga, and H. Suzuki, *Phys. Rev. B* **70**, 214434 (2004).
- [22] J. M. Hastings and L. M. Corliss, *Phys. Rev.* **126**, 556 (1962).
- [23] K. Dwight, *J. Appl. Phys.* **37**, 962 (1966).
- [24] R. Plumier, *J. Appl. Phys.* **39**, 635 (1968).
- [25] E. Winkler, S. Blanco Canosa, F. Rivadulla, M. A. Lopez-Quintela, J. Rivas, A. Caneiro, M. T. Causa, and M. Tovar, *Phys. Rev. B* **80**, 104418 (2009).
- [26] V. Kocsis, S. Bordacs, D. Varjas, K. Penc, A. Abouelsayed, C. A. Kuntscher, K. Ohgushi, Y. Tokura, and I. Kezsmarki, *Phys. Rev. B* **87**, 064416 (2013).
- [27] S. Kitani, M. Tachibana, N. Taira, and H. Kawaji, *Phys. Rev. B* **87**, 064402 (2013).
- [28] A. V. Pronin, M. Uhlarz, R. Beyer, T. Fischer, J. Wosnitza, B. P. Gorshunov, G. A. Komandin, A. S. Prokhorov, M. Dressel, A. A. Bush, and V. I. Torgashev, *Phys. Rev. B* **85**, 012101 (2012).
- [29] S. Bordacs, D. Varjas, I. Kezsmarki, G. Mihaly, L. Baldassarre, A. Abouelsayed, C. A. Kuntscher, K. Ohgushi, and Y. Tokura, *Phys. Rev. Lett.* **103**, 077205 (2009).
- [30] T. A. Kaplan and N. Menyuk, *Philos. Mag.* **87**, 3711 (2007).
- [31] S. Funahashi, Y. Morii, and H. R. Child, *J. Appl. Phys.* **61**, 4114 (1987).
- [32] See Supplemental Material at <http://link.aps.org/supplemental/10.1103/PhysRevB.97.064405> for XRD, XPS, and other relevant data, which include Refs. [18,19,54–57].
- [33] G. Kresse and J. Furthmüller, *Comput. Mater. Sci.* **6**, 15 (1996).
- [34] D. Porezag and M. R. Pederson, *Phys. Rev. B* **54**, 7830 (1996).
- [35] G. Kresse and D. Joubert, *Phys. Rev. B* **59**, 1758 (1999).
- [36] P. E. Blöchl, *Phys. Rev. B* **50**, 17953 (1994).
- [37] J. P. Perdew, K. Burke, and M. Ernzerhof, *Phys. Rev. Lett.* **77**, 3865 (1996).
- [38] C. Ederer and M. Komelj, *Phys. Rev. B* **76**, 064409 (2007).
- [39] S. L. Dudarev, G. A. Botton, S. Y. Savrasov, C. J. Humphreys, and A. P. Sutton, *Phys. Rev. B* **57**, 1505 (1998).
- [40] A. Togo and I. Tanaka, *Scr. Mater.* **108**, 1 (2015).
- [41] H. J. Monkhorst and J. D. Pack, *Phys. Rev. B* **13**, 5188 (1976).
- [42] C. Kittel, *Introduction to Solid State Physics* (Wiley, New York, 2008).

- [43] S. R. Pollack and K. R. Atkins, *Phys. Rev.* **125**, 1248 (1962).
- [44] N. Tristan, J. Hemberger, A. Krimmel, H. A. Krug von Nidda, V. Tsurkan, and A. Loidl, *Phys. Rev. B* **72**, 174404 (2005).
- [45] M. Ptak, M. Maczka, A. Gągor, A. Pikul, L. Macalik, and J. Hanuza, *J. Solid State Chem.* **201**, 270 (2013).
- [46] M. Balkanski, R. F. Wallis, and E. Haro, *Phys. Rev. B* **28**, 1928 (1983).
- [47] M. Ptak, M. Mączka, K. Hermanowicz, A. Pikul, and J. Hanuza, *J. Solid State Chem.* **199**, 295 (2013).
- [48] T. Kimura, *Annu. Rev. Condens. Matter Phys.* **3**, 93 (2012).
- [49] S. Dong, J.-M. Liu, S.-W. Cheong, and Z. Ren, *Adv. Phys.* **64**, 519 (2015).
- [50] Y. Tokura, S. Seki, and N. Nagaosa, *Rep. Prog. Phys.* **77**, 076501 (2014).
- [51] I. A. Sergienko and E. Dagotto, *Phys. Rev. B* **73**, 094434 (2006).
- [52] S. Dong, R. Yu, S. Yunoki, J. M. Liu, and E. Dagotto, *Phys. Rev. B* **78**, 155121 (2008).
- [53] T. Kimura, T. Goto, H. Shintani, K. Ishizaka, T. Arima, and Y. Tokura, *Nature (London)* **426**, 55 (2003).
- [54] C. Battistoni, J. L. Dormann, D. Fiorani, E. Paparazzo, and S. Viticoli, *Solid State Commun.* **39**, 581 (1981).
- [55] B. R. Strohmeier and D. M. Hercules, *J. Phys. Chem.* **88**, 4922 (1984).
- [56] J. C. Lashley, M. F. Hundley, A. Migliori, J. L. Sarrao, P. G. Pagliuso, T. W. Darling, M. Jaime, J. C. Cooley, W. L. Hults, L. Morales, D. J. Thoma, J. L. Smith, J. Boerio-Goates, B. F. Woodfield, G. R. Stewart, R. A. Fisher, and N. E. Phillips, *Cryogenics* **43**, 369 (2003).
- [57] S. Li, C. de la Cruz, Q. Huang, Y. Chen, J. W. Lynn, J. Hu, Y.-L. Huang, F.-C. Hsu, K.-W. Yeh, M.-K. Wu, and P. Dai, *Phys. Rev. B* **79**, 054503 (2009).